J. Appl. Comput. Mech., 12(1) (2026) 226-237
DOI: 10.22055/jacm.2025.48328.5152

ISSN: 2383-4536
jacm.scu.ac.ir

Shahid Chamran University of Ahvaz

Journal of Applied and Computational Mechanics

Research Paper

# Effects of Porosity and Nonlocality on the Damped Vibration Behaviors of Functionally Graded Rectangular Nanoplates on General Viscoelastic Medium

Le Truong Son[1], Pham Van Vinh[1,2]

[1] Department of Solid Mechanics, Le Quy Don Technical University, 236 Hoang Quoc Viet, Ha Noi, 10000, Viet Nam, Email: letruongson@lqdtu.edu.vn

[2] Institute of Physics and Mechanics, Peter the Great St. Petersburg Polytechnic University, 29 Polytechnicheskaya, Saint Petersburg, 195251, Russia, Email: fam.vv@edu.spbstu.ru

Received March 29 2025; Revised April 24 2025; Accepted for publication May 18 2025.
Corresponding author: L.T. Son (letruongson@lqdtu.edu.vn)


**Abstract.** This article presents an analytical framework for size-dependent damped vibration analysis of functionally graded nanoplates considering the effects of porosity. Two schemes of even and uneven porosity distributions are examined. The general viscoelastic foundations consist of four parameters that include two stiffness parameters and two viscosity coefficients. The small-scale effects are included in the proposed calculation model using nonlocal elasticity theory. A parametric study is carried out to demonstrate the effects of some geometric and material properties and nonlocal parameters on the damped vibration of the nanoplates. The outcomes of this study show that the stiffness parameters increase the damped frequency, but the damping coefficients reduce the damped frequency of the nanoplates.

**Keywords:** Nanoplates, Porosity, Viscoelastic foundation, Damped vibration, Nonlocal elasticity theory.

## 1. Introduction

Nanostructures, such as nanosized plates and beams, are widely used in advanced engineering applications, including nanoelectromechanical systems (NEMS), sensors, and biomedical devices [1, 2]. Understanding their vibration behavior is essential for ensuring their reliability and performance [3]. The vibrations of the nanoplates can be classified into free and damped vibrations. Free vibrations occur without external energy dissipation. These problems are used to determine the natural frequencies and mode shapes of the structures. On the other hand, damped vibrations involve energy loss due to internal material properties or external factors, which significantly affect the dynamic response of the structure. Studying damped vibrations of nanostructures is essential for precise forecasts and useful applications, as these structures function in situations where damping is present [4].

Functionally graded (FG) nanoplates are particularly useful due to their improved mechanical behavior [5-7]. However, these materials often contain pores due to manufacturing processes or intentional design choices [8-10]. The presence of porosity influences their stiffness and damping characteristics; therefore, it is necessary to develop accurate models that account for both material inhomogeneity and small-scale effects.

The mechanical behavior of local and nonlocal plates resting on elastic foundations has been extensively studied in structural mechanics. Several size-dependent theories were developed for the analysis of such structures, where the classical elasticity theory fails to capture small-scale effects. The nonlocal elasticity theory (NET), introduced by Eringen [11–13], assumes that the stress at a point depends on the strain through the solid body. This theory effectively captures long-range force interactions, and it is suitable for nanostructure analysis. Strain gradient theory incorporates higher-order spatial derivatives of strain into the constitutive relationships. Modified couple stress theory introduces an additional degree of freedom related to microrotation and corresponding couple stresses. This theory lies in the requirement of additional length-scale parameters and does not consider the nonlocal interaction. Modified strain gradient theory considers more higher-order strain gradient components into the strain energy, and it may compromise some generality in capturing complex material behavior. Lal et al. [14] studied the vibration and buckling behaviors of FG non-uniform circular plates resting on Winkler foundation. Sobhani et al. [15] analyzed the vibration of the imperfect graphene nanoplatelet reinforced nanocomposite conical shell lying on Winkler-Pasternak foundations. Jiang et al. [16] developed an approximate solution based on the Galerkin method for bending analysis of beams resting on nonlinear elastic foundation. Assie et al. [17] used unified shear deformation theories to study the bending of 2D FG plates with porosity and resting on elastic foundations. Ipek et al. [18] analyzed the buckling of nanocomposite plates on elastic foundations and embedded in thermal environments. Daikh et al. [19] examined the effects of various boundary conditions on the bending of FG sandwich nanoplates on the Pasternak foundation. Pour et al. [20] applied NET for the analysis of the circular bilayer graphene sheets on elastic foundation.

Published online: May 29 2025

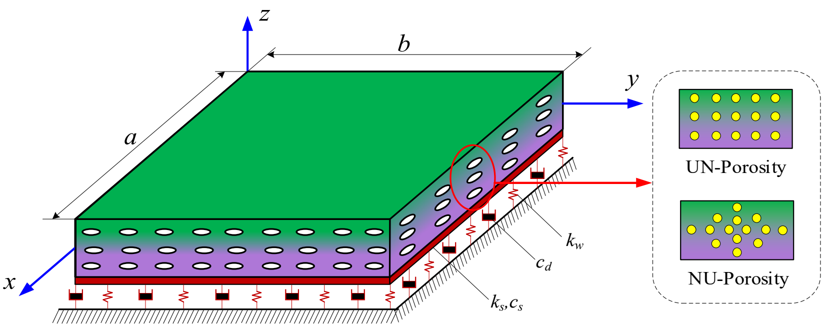


**Fig. 1.** FGSNP resting on general viscoelastic foundations.

Traditional foundation models such as the Winkler and Pasternak foundations provide simplified representations of the supporting medium. However, in many cases, structural elements interact with viscoelastic environments, where both elastic stiffness and damping effects need to be considered. To capture this behavior, viscoelastic foundation models have been introduced, incorporating both elastic and damping parameters. These models allow for a more realistic description of energy dissipation mechanisms in structures subjected to dynamic loads. Driz et al. [21] studied the dynamic response of FG plates with various graded patterns and resting on viscoelastic foundations. Tounsi et al. [22] investigated the influences of boundary conditions on the vibration characteristics of FG sandwich plates resting on three-parameter viscoelastic foundations. Van Vinh et al. [23] studied the viscoelastic vibration characteristics of FG sandwich plates on a general viscoelastic foundation. Zhang et al. [24] studied the wave propagation in carbon nanotube-reinforced nanocomposite doubly-curved shells on viscoelastic foundations. Foroutan et al. [25] examined the nonlinear vibration of the spiral stiffened multilayer FG shells on nonlinear viscoelastic foundations. Li et al. [26] analyzed the wave propagation is FG piezoelectric nanoplates on viscoelastic foundations. In this study, the effects of several porosity distributions on the damped vibration behaviors were also examined carefully.

Although previous studies have analyzed the effects of viscoelastic foundations on macroscale structures, there is still a need to extend these concepts to nanoscale structures, where small-scale effects and material gradation play a significant role. This study aims to develop an analytical framework for analyzing the damped vibrations of FG porous nanoplates (FGPNPs) resting on a general viscoelastic foundation. It is obvious that this is the first study about the dynamic response of the FGPNPs in contact with general viscoelastic foundations. The key novelty of this work lies in the combination of several advanced modeling aspects:

- The proposed foundation model includes simultaneously stiffness and damping components in both linear and shear layers.
- Two configurations of uniform and non-uniform porosity are considered, allowing for a more realistic representation of material imperfections.
- Small-scale effects are considered using the nonlocal elasticity theory.

By addressing these aspects, this study provides a more accurate and detailed understanding of the damped vibration behavior of FG porous nanoplates. The findings will be valuable for the design and optimization of nanodevices in engineering applications.

## 2. FGPNPs Resting on General Viscoelastic Foundations

A FGPNP is considered in this study, it has the dimensions of $a \times b \times h$ as presented in Fig. 1. The material components and their properties change smoothly through the thickness direction by the power law. The porosities are dispersed through the thickness direction in two forms: uniform (UN) and nonuniform (NU).

In the case of UN porosity distribution, the material properties are calculated as follows:

$$P(z) = P_c V_c + P_m V_m - \frac{e_0}{2}(P_c + P_m) \tag{1}$$

In the case of NU porosity distribution, the material properties are calculated as follows:

$$P(z) = P_c V_c + P_m V_m - \frac{e_0}{2}\left(1 - \frac{2|z|}{h}\right)(P_c + P_m) \tag{2}$$

where $e_0$ is a small coefficient, $0 \le e_0 \le 0.15$, that denotes the fraction of the porosity in the FGPNPs.

The FGPNPs are resting on a general viscoelastic foundation (GVF) with two layers including visco-Winkler and visco-Pasternak layers. The conversion reaction of the GVF can be expressed as follows:

$$R_f = k_w w - k_s \nabla^2 w + c_d \frac{\partial}{\partial t}(w) - c_s \frac{\partial}{\partial t}\left(\nabla^2 w\right) \tag{3}$$

where $w$ is the transverse displacement of the nanoplates, $k_w, k_s$ is the elastic parameters of visco-Winkler and visco-Pasternak layers, $c_d, c_s$ is the viscous coefficients of visco-Winkler and visco-Pasternak layers.

## 3. Theoretical Formulations

### 3.1. The nonlocal elasticity theory

To consider the small-scale effects in nano-scale dimension, the nonlocal elasticity theory of Eringen [11–13] is applied. The relationships between the nonlocal and local stresses of the solid body can be expressed as follows:

$$\left(1 - \mu \nabla^2\right) \sigma_{ij}^{nl} = \sigma_{ij}^{l} \tag{4}$$

where $\sigma_{ij}^{nl}, \sigma_{ij}^{l}$ are the nonlocal and local stresses of the solid body, respectively; $\nabla^2$ is the second Laplacian operator; and $\mu$ is the nonlocal parameters.

### 3.2. Constitutive relations

Based on the HSDT, the displacements of the nanoplates are described as follows:

$$\begin{aligned} U(x,y,z,t) &= u(x,y,t) - z\frac{\partial w_b(x,y,t)}{\partial x} - f(z)\frac{\partial w_s(x,y,t)}{\partial x} \\ V(x,y,z,t) &= v(x,y,t) - z\frac{\partial w_b(x,y,t)}{\partial y} - f(z)\frac{\partial w_s(x,y,t)}{\partial x} \\ W(x,y,z,t) &= w_b(x,y,t) + w_s(x,y,t) \end{aligned} \tag{5}$$

where $U, V, W$ are the displacements in $x, y, z$ directions; $u, v, w$ are the displacements of a points at the mid-plane of the FGPNPs, $w_b, w_s$ are the bending and shear parts of the transverse displacements of $w$. The function $f(z)$ is given as follows:

$$f(z) = z - \frac{h}{\pi}\sin\left(\frac{\pi z}{h}\right) \tag{6}$$

The non-zero terms of the strain field of the plates can be expressed as:

$$\begin{aligned} \varepsilon &= \varepsilon_0 + z\varepsilon_b + f(z)\varepsilon_s \\ \gamma &= g(z)\gamma_0 \end{aligned} \tag{7}$$

where,

$$\varepsilon = \begin{Bmatrix} \varepsilon_{xx} \\ \varepsilon_{yy} \\ \gamma_{xy} \end{Bmatrix}; \varepsilon_0 = \begin{Bmatrix} \dfrac{\partial u}{\partial x} \\ \dfrac{\partial v}{\partial y} \\ \dfrac{\partial v}{\partial x} + \dfrac{\partial u}{\partial y} \end{Bmatrix}; \varepsilon_b = \begin{Bmatrix} -\dfrac{\partial^2 w_b}{\partial x^2} \\ -\dfrac{\partial^2 w_b}{\partial y^2} \\ -2\dfrac{\partial^2 w_b}{\partial x \partial y} \end{Bmatrix}; \varepsilon_s = \begin{Bmatrix} -\dfrac{\partial^2 w_s}{\partial x^2} \\ -\dfrac{\partial^2 w_s}{\partial y^2} \\ -2\dfrac{\partial^2 w_s}{\partial x \partial y} \end{Bmatrix} \tag{8}$$

$$\gamma = \begin{Bmatrix} \gamma_{xz} \\ \gamma_{yz} \end{Bmatrix}; \gamma_0 = \begin{Bmatrix} \dfrac{\partial w_s}{\partial x} \\ \dfrac{\partial w_s}{\partial y} \end{Bmatrix} \tag{9}$$

$$g(z) = 1 - \frac{df(z)}{dz} = \cos\left(\frac{\pi z}{h}\right) \tag{10}$$

The nonlocal constitutive relation should be obtained as:

$$\left(1-\mu\nabla^2\right)\begin{Bmatrix} \sigma_{xx} \\ \sigma_{yy} \\ \tau_{xy} \\ \tau_{xz} \\ \tau_{yz} \end{Bmatrix} = \begin{bmatrix} \Phi_{11} & \Phi_{12} & 0 & 0 & 0 \\ \Phi_{12} & \Phi_{22} & 0 & 0 & 0 \\ 0 & 0 & \Phi_{66} & 0 & 0 \\ 0 & 0 & 0 & \Phi_{55} & 0 \\ 0 & 0 & 0 & 0 & \Phi_{44} \end{bmatrix} \begin{Bmatrix} \varepsilon_{xx} \\ \varepsilon_{yy} \\ \gamma_{xy} \\ \gamma_{xz} \\ \gamma_{yz} \end{Bmatrix} \tag{11}$$

where,

$$\Phi_{11} = \Phi_{22} = \frac{E(z)}{1-\nu^2(z)}; \Phi_{12} = \frac{\nu(z)E(z)}{1-\nu^2(z)}; \Phi_{44} = \Phi_{55} = \Phi_{66} = \frac{E(z)}{2[1+\nu(z)]} \tag{12}$$

### 3.3. The equations of motion

The equations of motion can be obtained using Hamilton's principle herein. The form below can be utilized:

$$\int_0^t (\delta\Pi + \delta F - \delta T)dt = 0 \tag{13}$$

The following formula can be used to determine the variation of the strain energy of the nanoplates:

$$\delta\Pi = \int_V \left(\sigma_{xx}\delta\varepsilon_{xx} + \sigma_{yy}\delta\varepsilon_{yy} + \tau_{xy}\delta\gamma_{xy} + \tau_{xz}\delta\gamma_{xz} + \tau_{yz}\delta\gamma_{yz}\right)dV \tag{14}$$

By integrating through the thickness of the nanoplates, the following formulation is achieved:

$$\delta\Pi = \int_S \left(\mathbf{N}^T\delta\varepsilon_0 + \mathbf{M}^T\delta\varepsilon_b + \mathbf{P}^T\delta\varepsilon_s + \mathbf{Q}\delta\gamma_0\right)dS \tag{15}$$

where $\mathbf{N}, \mathbf{M}, \mathbf{P}, \mathbf{Q}$ are the vectors of the nonlocal stress resultants that are defined as:

$$\mathbf{N} = \begin{Bmatrix} N_{xx} \\ N_{yy} \\ N_{xy} \end{Bmatrix}; \mathbf{M} = \begin{Bmatrix} M_{xx} \\ M_{yy} \\ M_{xy} \end{Bmatrix}; \mathbf{P} = \begin{Bmatrix} P_{xx} \\ P_{yy} \\ P_{xy} \end{Bmatrix}; \mathbf{Q} = \begin{Bmatrix} Q_{xz} \\ Q_{yz} \end{Bmatrix} \tag{16}$$

The nonlocal stress resultants $\mathbf{N}, \mathbf{M}, \mathbf{P}, \mathbf{Q}$ are calculated as follows:

$$\left(1-\mu\nabla^2\right)\begin{Bmatrix}\mathbf{N}\\ \mathbf{M}\\ \mathbf{P}\end{Bmatrix}=\begin{bmatrix}\mathbf{A} & \mathbf{B} & \mathbf{C}\\ \mathbf{B} & \mathbf{D} & \mathbf{E}\\ \mathbf{C} & \mathbf{E} & \mathbf{F}\end{bmatrix}\begin{Bmatrix}\varepsilon_0\\ \varepsilon_b\\ \varepsilon_s\end{Bmatrix};\left(1-\mu\nabla^2\right)\mathbf{Q}=\mathbf{A}_s\gamma_0 \tag{17}$$

$$\{\mathbf{A},\mathbf{B},\mathbf{C},\mathbf{D},\mathbf{E},\mathbf{F}\}=\int_{-h/2}^{h/2}\mathbf{D}_b\left\{1,z,f,z^2,zf,f^2\right\}dz;\ \mathbf{A}_s=\int_{-h/2}^{h/2}\mathbf{D}_s g^2 dz \tag{18}$$

$$\mathbf{D}_b=\begin{bmatrix}\Phi_{11} & \Phi_{12} & 0\\ \Phi_{12} & \Phi_{22} & 0\\ 0 & 0 & \Phi_{66}\end{bmatrix};\ \mathbf{D}_s=\begin{bmatrix}\Phi_{55} & 0\\ 0 & \Phi_{44}\end{bmatrix} \tag{19}$$

The variation of the work done by GVF is calculated as follows:

$$\begin{aligned}\delta F=\int_S\Bigg[&k_w(w_b+w_s)\delta(w_b+w_s)+k_s\left(\frac{\partial(w_b+w_s)}{\partial x}\frac{\partial\delta(w_b+w_s)}{\partial x}+\frac{\partial(w_b+w_s)}{\partial y}\frac{\partial\delta(w_b+w_s)}{\partial y}\right)\\ &+c_d(\dot{w}_b+\dot{w}_s)\delta(w_b+w_s)+c_s\left(\frac{\partial(\dot{w}_b+\dot{w}_s)}{\partial x}\frac{\partial\delta(w_b+w_s)}{\partial x}+\frac{\partial(\dot{w}_b+\dot{w}_s)}{\partial y}\frac{\partial\delta(w_b+w_s)}{\partial y}\right)\Bigg]dS\end{aligned} \tag{20}$$

The variation of the kinetic energy of the FGPNP can be calculated as follows:

$$\delta T=\delta\frac{1}{2}\int_V\rho(z)\left(\dot{U}^2+\dot{V}^2+\dot{W}^2\right)dV \tag{21}$$

After integrating through the thickness of the FGPNP, one gets:

$$\begin{aligned}\delta T=\int_S\Bigg[&I_0\left(\dot{u}\delta\dot{u}+\dot{v}\delta\dot{v}+(\dot{w}_b+\dot{w}_s)\delta(\dot{w}_b+\dot{w}_s)\right)+I_1\left(\dot{u}\frac{\partial\delta\dot{w}_b}{\partial x}+\delta\dot{u}\frac{\partial\dot{w}_b}{\partial x}+\dot{v}\frac{\partial\delta\dot{w}_b}{\partial y}+\delta\dot{v}\frac{\partial\dot{w}_b}{\partial y}\right)+I_2\left(\dot{u}\frac{\partial\delta\dot{w}_s}{\partial x}+\delta\dot{u}\frac{\partial\dot{w}_s}{\partial x}+\dot{v}\frac{\partial\delta\dot{w}_s}{\partial y}+\delta\dot{v}\frac{\partial\dot{w}_s}{\partial y}\right)\\ &+I_3\left(\frac{\partial\dot{w}_b}{\partial x}\frac{\partial\delta\dot{w}_b}{\partial x}+\frac{\partial\dot{w}_b}{\partial y}\frac{\partial\delta\dot{w}_b}{\partial y}\right)+I_4\left(\frac{\partial\dot{w}_b}{\partial x}\frac{\partial\delta\dot{w}_s}{\partial x}+\frac{\partial\dot{w}_s}{\partial x}\frac{\partial\delta\dot{w}_b}{\partial x}+\frac{\partial\dot{w}_b}{\partial y}\frac{\partial\delta\dot{w}_s}{\partial y}+\frac{\partial\dot{w}_s}{\partial y}\frac{\partial\delta\dot{w}_b}{\partial y}\right)+I_5\left(\frac{\partial\dot{w}_s}{\partial x}\frac{\partial\delta\dot{w}_s}{\partial x}+\frac{\partial\dot{w}_s}{\partial y}\frac{\partial\delta\dot{w}_s}{\partial y}\right)\Bigg]dS\end{aligned} \tag{22}$$

$$\{I_0,I_1,I_2,I_3,I_4,I_5\}=\int_{-h/2}^{h/2}\rho(z)\left\{1,-z,-f,z^2,zf,f^2\right\}dz \tag{23}$$

Substituting Eqs. (15), (20), and (22) into Eq. (13), and considering the relations in Eq. (17), the equations of motion in terms of the displacements are taken as follows:

$$\begin{aligned}\delta u:&-A_{11}\frac{\partial^2 u}{\partial x^2}-A_{12}\frac{\partial^2 v}{\partial x\partial y}+B_{11}\frac{\partial^3 w_b}{\partial x^3}+B_{12}\frac{\partial^3 w_b}{\partial x\partial y^2}+C_{11}\frac{\partial^3 w_s}{\partial x^3}+C_{12}\frac{\partial^3 w_s}{\partial x\partial y^2}\\ &-A_{33}\left(\frac{\partial^2 u}{\partial y^2}+\frac{\partial^2 v}{\partial x\partial y}\right)+2B_{33}\frac{\partial^3 w_b}{\partial x\partial y^2}+2C_{33}\frac{\partial^3 w_s}{\partial x\partial y^2}=\left(1-\mu\nabla^2\right)\left(-I_0\ddot{u}-I_1\frac{\partial\ddot{w}_b}{\partial x}-I_2\frac{\partial\ddot{w}_s}{\partial x}\right)\end{aligned} \tag{24}$$

$$\begin{aligned}\delta v:&-A_{12}\frac{\partial^2 u}{\partial x\partial y}-A_{22}\frac{\partial^2 v}{\partial y^2}+B_{12}\frac{\partial^3 w_b}{\partial x^2\partial y}+B_{22}\frac{\partial^3 w_b}{\partial y^3}+C_{12}\frac{\partial^3 w_s}{\partial x^2\partial y}+C_{22}\frac{\partial^3 w_s}{\partial y^3}\\ &-A_{33}\left(\frac{\partial^2 u}{\partial x\partial y}+\frac{\partial^2 v}{\partial x^2}\right)+2B_{33}\frac{\partial^3 w_b}{\partial x^2\partial y}+2C_{33}\left(\frac{\partial^3 w_s}{\partial x^2\partial y}\right)=\left(1-\mu\nabla^2\right)\left(-I_0\ddot{v}-I_1\frac{\partial\ddot{w}_b}{\partial y}-I_2\frac{\partial\ddot{w}_s}{\partial y}\right)\end{aligned} \tag{25}$$

$$\begin{aligned}\delta w_b:&-B_{11}\frac{\partial^3 u}{\partial x^3}-B_{12}\frac{\partial^3 v}{\partial x^2\partial y}+D_{11}\frac{\partial^4 w_b}{\partial x^4}+2D_{12}\frac{\partial^4 w_b}{\partial x^2\partial y^2}+E_{11}\frac{\partial^4 w_s}{\partial x^4}+2E_{12}\frac{\partial^4 w_s}{\partial x^2\partial y^2}+4D_{33}\frac{\partial^4 w_b}{\partial x^2\partial y^2}\\ &-2B_{33}\left(\frac{\partial^3 u}{\partial x\partial y^2}+\frac{\partial^3 v}{\partial x^2\partial y}\right)+4E_{33}\left(\frac{\partial^4 w_s}{\partial x^2\partial y^2}\right)-B_{12}\frac{\partial^3 u}{\partial x\partial y^2}-B_{22}\frac{\partial^3 v}{\partial y^3}+D_{22}\frac{\partial^4 w_b}{\partial y^4}+E_{22}\frac{\partial^4 w_s}{\partial y^4}+\\ &\left(1-\mu\nabla^2\right)\left(k_x(w_b+w_s)-k_s\nabla^2(w_b+w_s)+c_d(\dot{w}_b+\dot{w}_s)-c_s\nabla^2(\dot{w}_b+\dot{w}_s)\right)\\ &=\left(1-\mu\nabla^2\right)\left[-I_0(\ddot{w}_b+\ddot{w}_s)+I_1\left(\frac{\partial\ddot{u}}{\partial x}+\frac{\partial\ddot{v}}{\partial y}\right)+I_3\nabla^2\ddot{w}_b+I_4\nabla^2\ddot{w}_s\right]\end{aligned} \tag{26}$$

$$\begin{aligned}\delta w_s:&-C_{11}\frac{\partial^3 u}{\partial x^3}-C_{12}\frac{\partial^3 v}{\partial x^2\partial y}+E_{11}\frac{\partial^4 w_b}{\partial x^4}+2E_{12}\frac{\partial^4 w_b}{\partial x^2\partial y^2}+F_{11}\frac{\partial^4 w_s}{\partial x^4}+2F_{12}\frac{\partial^4 w_s}{\partial x^2\partial y^2}+4E_{33}\frac{\partial^4 w_b}{\partial x^2\partial y^2}-As_{11}\frac{\partial^2 w_s}{\partial y^2}\\ &-2C_{33}\left(\frac{\partial^3 u}{\partial x\partial y^2}+\frac{\partial^3 v}{\partial x^2\partial y}\right)+4F_{33}\left(\frac{\partial^4 w_s}{\partial x^2\partial y^2}\right)-C_{12}\frac{\partial^3 u}{\partial x\partial y^2}-C_{22}\frac{\partial^3 v}{\partial y^3}+E_{22}\frac{\partial^4 w_b}{\partial y^4}+F_{22}\frac{\partial^4 w_s}{\partial y^4}-As_{22}\frac{\partial^2 w_s}{\partial x^2}\\ &+\left(1-\mu\nabla^2\right)\left(k_x(w_b+w_s)-k_s\nabla^2(w_b+w_s)+c_d(\dot{w}_b+\dot{w}_s)-c_s\nabla^2(\dot{w}_b+\dot{w}_s)\right)\\ &=\left(1-\mu\nabla^2\right)\left[-I_0(\ddot{w}_b+\ddot{w}_s)+I_2\left(\frac{\partial\ddot{u}}{\partial x}+\frac{\partial\ddot{v}}{\partial y}\right)+I_4\nabla^2\ddot{w}_b+I_5\nabla^2\ddot{w}_s\right]\end{aligned} \tag{27}$$

## 4. Solution Method

The Navier solution is used to solve the equations of motion of a simply supported FGPNP. The displacements are given as follows:

$$\begin{Bmatrix} u \\ v \\ w_b \\ w_s \end{Bmatrix} = \sum_{n=1}^{\infty}\sum_{m=1}^{\infty}\begin{Bmatrix} U_{mn}\cos(\alpha x)\sin(\beta y) \\ V_{mn}\sin(\alpha x)\cos(\beta y) \\ W_{mn}^{b}\sin(\alpha x)\sin(\beta y) \\ W_{mn}^{s}\sin(\alpha x)\sin(\beta y) \end{Bmatrix} e^{\lambda t} \tag{28}$$

where $\alpha = \pi m/a, \beta = \pi n/b$, and $\mathbf{d} = \{U_{mn}, V_{mn}, W_{mn}^{b}, W_{mn}^{s}\}$ are the vector of the unknown coefficients, $\lambda$ is complex eigenvalue. By substituting Eq. (28) into Eqs. (24) - (27), and then rearrange into the matrix form, one gets:

$$\left(\mathbf{K} + \lambda\mathbf{C} + \lambda^2\mathbf{M}\right)\mathbf{d} = 0 \tag{29}$$

By solving this equation, one gets the eigenvalues and eigenvectors. The complex eigenvalues consist of two parts, which are imaginary and real parts of the frequency of the FGPNPs. They can be expanded as follows:

$$\lambda_{1,2} = -\omega\left(\xi \mp i\sqrt{1-\xi^2}\right) \tag{30}$$

For underdamped vibration, the frequency of damped vibration $\omega_d$ of the FGPNPs can be expressed as:

$$\omega_d = \omega\sqrt{1-\xi^2} \tag{31}$$

where $\omega$ is the frequency of undamped vibration of the FGPNPs, $\xi$ is the damping ratio, which depends on the construction of the system.

The elements $k_{ij}, c_{ij}, m_{ij}$ of $\mathbf{K}, \mathbf{C}, \mathbf{M}$ are given below:

$$\begin{aligned}
&k_{11} = A_{11}\alpha^2 + A_{33}\beta^2;\ k_{12} = k_{21} = (A_{12} + A_{33})\beta\alpha;\ k_{13} = k_{31} = -B_{11}\alpha^3 - (B_{12} + 2B_{33})\beta^2\alpha \\
&k_{14} = k_{41} = -C_{11}\alpha^3 - (C_{12} + 2C_{33})\beta^2\alpha;\ k_{22} = A_{22}\beta^2 + A_{33}\alpha^2;\ k_{23} = k_{32} = -B_{22}\beta^3 - (B_{12} + 2B_{33})\alpha^2\beta \\
&k_{24} = k_{42} = -C_{22}\beta^3 - 2\left(C_{33} + \frac{C_{12}}{2}\right)\alpha^2\beta;\ k_{33} = D_{11}\alpha^4 + 4\left(D_{33} + \frac{D_{12}}{2}\right)\beta^2\alpha^2 + D_{22}\beta^4 + k_f \\
&k_{34} = k_{43} = E_{11}\alpha^4 + 2(E_{12} + 2E_{33})\beta^2\alpha^2 + E_{22}\beta^4 + k_f \\
&k_{44} = F_{11}\alpha^4 + \left((2F_{12} + 4F_{33})\beta^2 + As_{11}\right)\alpha^2 + \beta^2\left(F_{22}\beta^2 + As_{22}\right) + k_f
\end{aligned} \tag{32}$$

$$k_f = \left[1 + \mu\left(\alpha^2 + \beta^2\right)\right]\left[k_w + k_s\left(\alpha^2 + \beta^2\right)\right] \tag{33}$$

$$\begin{aligned}
&c_{11} = c_{12} = c_{13} = c_{14} = 0;\ c_{22} = c_{23} = c_{24} = 0; \\
&c_{33} = \left[1 + \mu\left(\alpha^2 + \beta^2\right)\right]\left[\left(\alpha^2 + \beta^2\right)c_s + c_d\right]; \\
&c_{34} = c_{43} = c_{44} = c_{33}.
\end{aligned} \tag{34}$$

$$\begin{aligned}
&m_{11} = I_0\left[1 + \mu\left(\alpha^2 + \beta^2\right)\right];\ m_{12} = m_{21} = 0;\ m_{13} = m_{31} = I_1\alpha\left[1 + \mu\left(\alpha^2 + \beta^2\right)\right];\ m_{14} = m_{41} = I_2\alpha\left[1 + \mu\left(\alpha^2 + \beta^2\right)\right]; \\
&m_{22} = I_0\left[1 + \mu\left(\alpha^2 + \beta^2\right)\right];\ m_{23} = m_{32} = I_1\beta\left[1 + \mu\left(\alpha^2 + \beta^2\right)\right];\ m_{34} = m_{43} = \left[\left(\alpha^2 + \beta^2\right)I_4 + I_0\right]\left[1 + \mu\left(\alpha^2 + \beta^2\right)\right]; \\
&m_{33} = \left[\left(\alpha^2 + \beta^2\right)I_3 + I_0\right]\left[1 + \mu\left(\alpha^2 + \beta^2\right)\right];\ m_{24} = m_{42} = I_2\beta\left[1 + \mu\left(\alpha^2 + \beta^2\right)\right];\ m_{44} = \left[\left(\alpha^2 + \beta^2\right)I_5 + I_0\right]\left[1 + \mu\left(\alpha^2 + \beta^2\right)\right]
\end{aligned} \tag{35}$$

## 5. Results and Discussions

In this section, several comparison studies are carried out to demonstrate the accuracy and efficiency of the present algorithm in predicting the damped vibration behaviors of the FG porous nanoplates on viscoelastic foundation. A deep parametric study is presented to demonstrate the effects of some parameters on the damped vibration characteristics of the FG porous plates.

### 5.1. Validation study

First, a square FG plate is examined to validate the accuracy of the present algorithm for predicting vibration behaviors of the plates with porosity. The plates are made of $Al/Al_2O_3$ with UN porosity distribution, the dimensions are $a/h = 10$ and $a/h = 20$. Their material properties are: $E_c = 380$ GPa, $\rho_c = 3800$ kg/m$^3$, $\nu_c = 0.3$, $E_m = 70$ GPa, $\rho_m = 2707$ kg/m$^3$, $\nu_m = 0.3$.

The nondimensional frequencies of the plates are calculated as follows:

$$\hat{\omega} = \omega h\sqrt{\rho_c / E_c} \tag{36}$$

In this example, it is noticed that the Poisson's ratio is independent with the porosity. The numerical results are compared with those of Mouaici et al. [27] and Wang et al. [28] as presented in Table 1. The comparison shows that the present results are very close to the published solutions. Therefore, the proposed calculation can be used to analysis of the structures with porosity.

To validate the accuracy of the proposed algorithm, the damped vibration behavior of an FG porous plates resting on viscoelastic foundations. The plate is made of $ZrO_2/Al$ with their material properties are $E_c = 200$ GPa, $\rho_c = 5700$ kg/m$^3$, $\nu_c = 0.3$, $E_m = 70$ GPa, $\rho_m = 2707$ kg/m$^3$, $\nu_m = 0.3$.

**Table 1.** Comparison of nondimensional frequencies of FG porous plates.

| $e_0$ | References | $p$ = 1 | | $p$ = 4 | | $p$ = 10 | |
|---|---|---|---|---|---|---|---|
| | | $a/h$ = 10 | $a/h$ = 20 | $a/h$ = 10 | $a/h$ = 20 | $a/h$ = 10 | $a/h$ = 20 |
| | Mouaici et al. [27] | 0.0432 | 0.0110 | 0.0353 | 0.0090 | 0.0336 | 0.0087 |
| 0.1 | Wang et al. [28] | 0.0433 | 0.0111 | 0.0354 | 0.0091 | 0.0337 | 0.0087 |
| | Present work | 0.0432 | 0.0111 | 0.0353 | 0.0091 | 0.0336 | 0.0087 |
| | Mouaici et al. [27] | 0.0418 | 0.0106 | 0.0304 | 0.0078 | 0.0285 | 0.0074 |
| 0.2 | Wang et al. [28] | 0.0419 | 0.0107 | 0.0306 | 0.0078 | 0.0287 | 0.0074 |
| | Present work | 0.0419 | 0.0107 | 0.0304 | 0.0078 | 0.0285 | 0.0074 |

**Table 2.** Comparison of damped frequency of FG porous plates on viscoelastic foundation ($K_w = 100$, $K_s = 50$).

| $C_d$ | References | $C_S$ | | | | | |
|---|---|---|---|---|---|---|---|
| | | 0 | 1 | 2 | 3 | 4 | 5 |
| 0 | Ghazwani et al. [29] | 1.39169 | 1.39082 | 1.38820 | 1.38382 | 1.37768 | 1.36974 |
| | Present work | 1.39167 | 1.39080 | 1.38818 | 1.38381 | 1.37766 | 1.36972 |
| 1 | Ghazwani et al. [29] | 1.39146 | 1.38969 | 1.38617 | 1.38089 | 1.37383 | 1.36495 |
| | Present work | 1.39144 | 1.38967 | 1.38616 | 1.38088 | 1.37381 | 1.36494 |
| 2 | Ghazwani et al. [29] | 1.39077 | 1.38810 | 1.38368 | 1.37749 | 1.36950 | 1.35968 |
| | Present work | 1.39075 | 1.38809 | 1.38367 | 1.37748 | 1.36949 | 1.35967 |
| 3 | Ghazwani et al. [29] | 1.38962 | 1.38606 | 1.38073 | 1.37362 | 1.36469 | 1.35392 |
| | Present work | 1.38960 | 1.38604 | 1.38071 | 1.37360 | 1.36468 | 1.35391 |
| 4 | Ghazwani et al. [29] | 1.38801 | 1.38354 | 1.37730 | 1.36926 | 1.35940 | 1.34766 |
| | Present work | 1.38799 | 1.38353 | 1.37729 | 1.36925 | 1.35938 | 1.34764 |

**Table 3.** Comparison of frequencies of isotropic nanoplates.

| $a/h$ | $b/a$ | References | $\mu$ = 0 | $\mu$ = 1 | $\mu$ = 2 | $\mu$ = 3 | $\mu$ = 4 | $\mu$ = 5 |
|---|---|---|---|---|---|---|---|---|
| 10 | 1 | Zenkour [30] and Hoa et al. [31] | 0.093028 | 0.085015 | 0.078769 | 0.073725 | 0.069540 | 0.065996 |
| | | Present work | 0.093037 | 0.085023 | 0.078778 | 0.073733 | 0.069548 | 0.066003 |
| | 2 | Zenkour [30] and Hoa et al. [31] | 0.058883 | 0.055556 | 0.052735 | 0.050305 | 0.048182 | 0.046308 |
| | | Present work | 0.058888 | 0.055560 | 0.052740 | 0.050309 | 0.048186 | 0.046312 |
| 20 | 1 | Zenkour [30] and Hoa et al. [31] | 0.023864 | 0.021808 | 0.020206 | 0.018912 | 0.017839 | 0.016929 |
| | | Present work | 0.023865 | 0.021809 | 0.020207 | 0.018913 | 0.017840 | 0.016930 |
| | 2 | Zenkour [30] and Hoa et al. [31] | 0.014963 | 0.014119 | 0.013402 | 0.012785 | 0.012245 | 0.011769 |
| | | Present work | 0.014966 | 0.014120 | 0.013403 | 0.012786 | 0.012246 | 0.011770 |

The porosity distributed through the thickness direction with uniform scheme, and the effective material properties are calculated as follows:

$$\begin{aligned} E(z) &= \left[E_m + (E_c - E_m)V_c(z)\right]\left[1 - e_0\right] \\ \rho(z) &= \left[\rho_m + (\rho_c - \rho_m)V_c(z)\right]\left[1 - e_0\right] \\ \nu(z) &= \left[\nu_m + (\nu_c - \nu_m)V_c(z)\right]\left[1 - e_0\right] \end{aligned} \tag{37}$$

In this comparison, the parameters of the plates are $a = b = 1$ m, $h = 0.1a$, $p = 1$, $e_0 = 0.2$. The boundary conditions are simply support at all edges of the plates. The dimensionless quantities are calculated by:

$$\begin{aligned} &\Omega_d = \omega_d h_0\sqrt{\frac{10^2\rho_c}{E_c}};\ \Omega_{\mathrm{Re}} = \mathrm{Re}(s)\cdot h_0\sqrt{\frac{10^2\rho_c}{E_c}};K_w = \frac{k_w a^4}{D_c};\ K_s = \frac{k_s a^2}{D_c}; \\ &C_d = c_d\sqrt{\frac{1}{\rho_c D_c h_0}};C_s = c_s\frac{1}{\pi^2 h_0^2}\sqrt{\frac{1}{\rho_c D_c h_0}};D_c = \frac{E_c h_0^3}{12(1-\nu^2)};h_0 = \frac{a}{10} \end{aligned} \tag{38}$$

The present results are compared with the solutions of Ghazwani et al. [29] as presented in Table 2. The comparison shows that the present results are in good agreement with the published results. This means that the proposed algorithm is suitable for analysis of FG porous plates.

Third, a rectangular isotropic homogeneous nanoplates $Al_2O_3$ with the width of $a = 10$ nm is studied to validate the accuracy of the present calculation for analysis of the nanoplates. The nondimensional frequencies of the nanoplates are calculated by:

$$\varpi = \omega h\sqrt{\frac{\rho_c}{G_c}};\ G = \frac{E_c}{2(1+\nu_c)} \tag{39}$$

The comparison between present results and the solutions of Zenkour [30] and Hoa et al. [31] are given in Table 3. It can be concluded that the present algorithm is suitable for predicting the vibration behaviors of the nanoplates.

**Table 4.** Dimensionless damped frequency $\Omega_d$ of the square FGPNPs ($K_w = 10,\ K_s = 5,\ \mu = 0,\ p = 1$).

| $C_d$ | $C_S$ | Perfect | UN porosity | | | NU porosity | | |
|---|---|---|---|---|---|---|---|---|
| | | $e_0 = 0.0$ | $e_0 = 0.05$ | $e_0 = 0.1$ | $e_0 = 0.15$ | $e_0 = 0.05$ | $e_0 = 0.1$ | $e_0 = 0.15$ |
| 0 | 0 | 0.6783 | 0.6777 | 0.6772 | 0.6767 | 0.6814 | 0.6846 | 0.6880 |
| | 1 | 0.6783 | 0.6776 | 0.6772 | 0.6767 | 0.6814 | 0.6846 | 0.6880 |
| | 2 | 0.6782 | 0.6776 | 0.6771 | 0.6766 | 0.6813 | 0.6845 | 0.6879 |
| | 5 | 0.6777 | 0.6770 | 0.6764 | 0.6759 | 0.6808 | 0.6840 | 0.6873 |
| | 10 | 0.6759 | 0.6750 | 0.6742 | 0.6734 | 0.6789 | 0.6820 | 0.6852 |
| 1 | 0 | 0.6777 | 0.6770 | 0.6764 | 0.6759 | 0.6807 | 0.6839 | 0.6873 |
| | 1 | 0.6774 | 0.6767 | 0.6761 | 0.6755 | 0.6805 | 0.6837 | 0.6870 |
| | 2 | 0.6771 | 0.6764 | 0.6757 | 0.6751 | 0.6801 | 0.6833 | 0.6866 |
| | 5 | 0.6759 | 0.6750 | 0.6742 | 0.6734 | 0.6788 | 0.6820 | 0.6852 |
| | 10 | 0.6729 | 0.6717 | 0.6705 | 0.6692 | 0.6757 | 0.6787 | 0.6817 |
| 2 | 0 | 0.6758 | 0.6750 | 0.6742 | 0.6733 | 0.6788 | 0.6819 | 0.6852 |
| | 1 | 0.6753 | 0.6744 | 0.6735 | 0.6726 | 0.6783 | 0.6814 | 0.6846 |
| | 2 | 0.6748 | 0.6738 | 0.6728 | 0.6718 | 0.6777 | 0.6808 | 0.6839 |
| | 5 | 0.6728 | 0.6716 | 0.6704 | 0.6691 | 0.6756 | 0.6786 | 0.6817 |
| | 10 | 0.6686 | 0.6669 | 0.6651 | 0.6632 | 0.6712 | 0.6739 | 0.6768 |
| 5 | 0 | 0.6628 | 0.6605 | 0.6580 | 0.6552 | 0.6652 | 0.6676 | 0.6702 |
| | 1 | 0.6616 | 0.6591 | 0.6564 | 0.6534 | 0.6639 | 0.6663 | 0.6687 |
| | 2 | 0.6603 | 0.6576 | 0.6548 | 0.6515 | 0.6625 | 0.6648 | 0.6672 |
| | 5 | 0.6560 | 0.6529 | 0.6495 | 0.6456 | 0.6581 | 0.6601 | 0.6623 |
| | 10 | 0.6479 | 0.6439 | 0.6393 | 0.6341 | 0.6495 | 0.6512 | 0.6529 |
| 10 | 0 | 0.6142 | 0.6061 | 0.5968 | 0.5857 | 0.6141 | 0.6139 | 0.6136 |
| | 1 | 0.6115 | 0.6031 | 0.5933 | 0.5817 | 0.6113 | 0.6109 | 0.6104 |
| | 2 | 0.6087 | 0.6000 | 0.5898 | 0.5777 | 0.6083 | 0.6079 | 0.6072 |
| | 5 | 0.6000 | 0.5902 | 0.5787 | 0.5650 | 0.5992 | 0.5982 | 0.5970 |
| | 10 | 0.5842 | 0.5723 | 0.5583 | 0.5414 | 0.5825 | 0.5806 | 0.5783 |

**Table 5.** The relative damping ratio $\xi$ of the square FGPNPs ($K_w = 10,\ K_s = 5,\ \mu = 0,\ p = 1$).

| $C_d$ | $C_S$ | Perfect | UN porosity | | | NU porosity | | |
|---|---|---|---|---|---|---|---|---|
| | | $e_0 = 0.0$ | $e_0 = 0.05$ | $e_0 = 0.1$ | $e_0 = 0.15$ | $e_0 = 0.05$ | $e_0 = 0.1$ | $e_0 = 0.15$ |
| 0 | 0 | 0 | 0 | 0 | 0 | 0 | 0 | 0 |
| | 1 | 0.0084 | 0.0088 | 0.0093 | 0.0099 | 0.0086 | 0.0087 | 0.0089 |
| | 2 | 0.0168 | 0.0177 | 0.0187 | 0.0198 | 0.0171 | 0.0175 | 0.0179 |
| | 5 | 0.0419 | 0.0441 | 0.0467 | 0.0494 | 0.0428 | 0.0437 | 0.0446 |
| | 10 | 0.0838 | 0.0883 | 0.0933 | 0.0989 | 0.0855 | 0.0874 | 0.0893 |
| 1 | 0 | 0.0424 | 0.0447 | 0.0473 | 0.0501 | 0.0433 | 0.0443 | 0.0452 |
| | 1 | 0.0508 | 0.0536 | 0.0566 | 0.0600 | 0.0519 | 0.0530 | 0.0542 |
| | 2 | 0.0592 | 0.0624 | 0.0659 | 0.0699 | 0.0604 | 0.0617 | 0.0631 |
| | 5 | 0.0843 | 0.0889 | 0.0939 | 0.0996 | 0.0861 | 0.0879 | 0.0899 |
| | 10 | 0.1262 | 0.1330 | 0.1406 | 0.1490 | 0.1289 | 0.1316 | 0.1345 |
| 2 | 0 | 0.0849 | 0.0895 | 0.0945 | 0.1002 | 0.0867 | 0.0885 | 0.0905 |
| | 1 | 0.0933 | 0.0983 | 0.1039 | 0.1101 | 0.0952 | 0.0973 | 0.0994 |
| | 2 | 0.1016 | 0.1071 | 0.1132 | 0.1200 | 0.1038 | 0.1060 | 0.1083 |
| | 5 | 0.1268 | 0.1336 | 0.1412 | 0.1497 | 0.1294 | 0.1322 | 0.1351 |
| | 10 | 0.1687 | 0.1778 | 0.1878 | 0.1991 | 0.1722 | 0.1759 | 0.1798 |
| 5 | 0 | 0.2122 | 0.2237 | 0.2363 | 0.2505 | 0.2167 | 0.2213 | 0.2262 |
| | 1 | 0.2206 | 0.2325 | 0.2457 | 0.2604 | 0.2252 | 0.2300 | 0.2351 |
| | 2 | 0.2290 | 0.2413 | 0.2550 | 0.2703 | 0.2338 | 0.2388 | 0.2440 |
| | 5 | 0.2541 | 0.2678 | 0.2830 | 0.3000 | 0.2594 | 0.2650 | 0.2708 |
| | 10 | 0.2960 | 0.3119 | 0.3296 | 0.3494 | 0.3022 | 0.3087 | 0.3155 |
| 10 | 0 | 0.4244 | 0.4473 | 0.4727 | 0.5010 | 0.4333 | 0.4426 | 0.4523 |
| | 1 | 0.4328 | 0.4561 | 0.4820 | 0.5109 | 0.4419 | 0.4513 | 0.4613 |
| | 2 | 0.4412 | 0.4650 | 0.4913 | 0.5208 | 0.4504 | 0.4601 | 0.4702 |
| | 5 | 0.4663 | 0.4915 | 0.5193 | 0.5505 | 0.4761 | 0.4863 | 0.4970 |
| | 10 | 0.5082 | 0.5356 | 0.5660 | 0.5999 | 0.5189 | 0.5300 | 0.5416 |

### 5.2. Numerical results and discussions

To demonstrate how different parameters impact the vibration behaviors of the FGPNPs, this section will carry out extensive parametric research, with a focus on the influence of the novel foundation model. The FGPNPs are made from a mixture of metal and ceramic phases with their properties of $E_m = 1.44$ GPa, $\rho_m = 1220\ \mathrm{kg/m^3}$, $\nu_m = 0.3$, $E_c = 14.4$ GPa, $\rho_c = 12200\ \mathrm{kg/m^3}$, $\nu_c = 0.38$ [32]. The dimensions of the nanoplates are $a = b = 10$ nm, $h = a/10$, and subjected to simply support at all edges. The dimensionless quantities are calculated by:

$$\begin{aligned} &\Omega_d = \omega_d h_0 \sqrt{\frac{10^2 \rho_c}{E_c}};\ \Omega_{\mathrm{Re}} = \mathrm{Re}(s)\cdot h_0 \sqrt{\frac{10^2 \rho_c}{E_c}};K_w = \frac{k_w a^4}{D_c};\ K_s = \frac{k_s a^2}{D_c};\\ &C_d = c_d \pi^4 \sqrt{\frac{1}{\rho_c D_c h_0}};C_s = c_s \frac{\pi^4}{h_0^2}\sqrt{\frac{1}{\rho_c D_c h_0}};D_c = \frac{E_c h_0^3}{12(1-\nu^2)};h_0 = \frac{a}{10} \end{aligned} \tag{40}$$

**Table 6.** Dimensionless damped frequency $\Omega_d$ of the square FGPNPs ($K_w = 10,\ K_s = 5,\ \mu = 4,\ p = 1$).

| $C_d$ | $C_s$ | Perfect | UN porosity | | | NU porosity | | |
|---|---|---|---|---|---|---|---|---|
| | | $e_0 = 0.0$ | $e_0 = 0.05$ | $e_0 = 0.1$ | $e_0 = 0.15$ | $e_0 = 0.05$ | $e_0 = 0.1$ | $e_0 = 0.15$ |
| 0 | 0 | 0.5840 | 0.5874 | 0.5913 | 0.5956 | 0.5878 | 0.5918 | 0.5960 |
| | 1 | 0.5839 | 0.5873 | 0.5912 | 0.5956 | 0.5878 | 0.5918 | 0.5960 |
| | 2 | 0.5839 | 0.5872 | 0.5911 | 0.5955 | 0.5877 | 0.5917 | 0.5959 |
| | 5 | 0.5833 | 0.5866 | 0.5904 | 0.5947 | 0.5871 | 0.5911 | 0.5952 |
| | 10 | 0.5812 | 0.5843 | 0.5879 | 0.5919 | 0.5849 | 0.5888 | 0.5928 |
| 1 | 0 | 0.5833 | 0.5866 | 0.5904 | 0.5947 | 0.5871 | 0.5910 | 0.5952 |
| | 1 | 0.5830 | 0.5862 | 0.5900 | 0.5942 | 0.5868 | 0.5907 | 0.5948 |
| | 2 | 0.5826 | 0.5858 | 0.5896 | 0.5937 | 0.5864 | 0.5903 | 0.5944 |
| | 5 | 0.5812 | 0.5843 | 0.5878 | 0.5918 | 0.5849 | 0.5888 | 0.5928 |
| | 10 | 0.5777 | 0.5804 | 0.5835 | 0.5870 | 0.5812 | 0.5849 | 0.5888 |
| 2 | 0 | 0.5811 | 0.5842 | 0.5878 | 0.5918 | 0.5848 | 0.5887 | 0.5928 |
| | 1 | 0.5805 | 0.5836 | 0.5871 | 0.5909 | 0.5842 | 0.5881 | 0.5921 |
| | 2 | 0.5799 | 0.5829 | 0.5863 | 0.5901 | 0.5835 | 0.5874 | 0.5913 |
| | 5 | 0.5776 | 0.5804 | 0.5835 | 0.5870 | 0.5812 | 0.5849 | 0.5887 |
| | 10 | 0.5727 | 0.5749 | 0.5774 | 0.5802 | 0.5760 | 0.5794 | 0.5830 |
| 5 | 0 | 0.5660 | 0.5675 | 0.5692 | 0.5710 | 0.5690 | 0.5721 | 0.5753 |
| | 1 | 0.5645 | 0.5659 | 0.5674 | 0.5690 | 0.5674 | 0.5705 | 0.5736 |
| | 2 | 0.5629 | 0.5642 | 0.5655 | 0.5668 | 0.5658 | 0.5688 | 0.5719 |
| | 5 | 0.5580 | 0.5586 | 0.5593 | 0.5600 | 0.5606 | 0.5633 | 0.5661 |
| | 10 | 0.5484 | 0.5480 | 0.5475 | 0.5467 | 0.5506 | 0.5528 | 0.5551 |
| 10 | 0 | 0.5081 | 0.5031 | 0.4971 | 0.4897 | 0.5083 | 0.5084 | 0.5083 |
| | 1 | 0.5048 | 0.4995 | 0.4930 | 0.4850 | 0.5049 | 0.5048 | 0.5045 |
| | 2 | 0.5015 | 0.4957 | 0.4888 | 0.4802 | 0.5013 | 0.5010 | 0.5006 |
| | 5 | 0.4909 | 0.4838 | 0.4753 | 0.4648 | 0.4902 | 0.4893 | 0.4882 |
| | 10 | 0.4714 | 0.4618 | 0.4502 | 0.4358 | 0.4696 | 0.4676 | 0.4652 |

**Table 7.** The relative damping ratio $\xi$ of the square FGPNPs ($K_w = 10,\ K_s = 5,\ \mu = 4,\ p = 1$).

| $C_d$ | $C_s$ | Perfect | UN porosity | | | NU porosity | | |
|---|---|---|---|---|---|---|---|---|
| | | $e_0 = 0.0$ | $e_0 = 0.05$ | $e_0 = 0.1$ | $e_0 = 0.15$ | $e_0 = 0.05$ | $e_0 = 0.1$ | $e_0 = 0.15$ |
| 0 | 0 | 0 | 0 | 0 | 0 | 0 | 0 | 0 |
| | 1 | 0.0097 | 0.0102 | 0.0107 | 0.0112 | 0.0099 | 0.0101 | 0.0103 |
| | 2 | 0.0195 | 0.0204 | 0.0214 | 0.0225 | 0.0198 | 0.0202 | 0.0206 |
| | 5 | 0.0487 | 0.0509 | 0.0534 | 0.0562 | 0.0496 | 0.0505 | 0.0515 |
| | 10 | 0.0973 | 0.1019 | 0.1069 | 0.1124 | 0.0991 | 0.1011 | 0.1031 |
| 1 | 0 | 0.0493 | 0.0516 | 0.0541 | 0.0569 | 0.0502 | 0.0512 | 0.0522 |
| | 1 | 0.0590 | 0.0618 | 0.0648 | 0.0682 | 0.0601 | 0.0613 | 0.0625 |
| | 2 | 0.0688 | 0.0720 | 0.0755 | 0.0794 | 0.0701 | 0.0714 | 0.0728 |
| | 5 | 0.0980 | 0.1025 | 0.1076 | 0.1131 | 0.0998 | 0.1017 | 0.1037 |
| | 10 | 0.1466 | 0.1535 | 0.1610 | 0.1693 | 0.1494 | 0.1523 | 0.1553 |
| 2 | 0 | 0.0986 | 0.1032 | 0.1083 | 0.1138 | 0.1005 | 0.1024 | 0.1044 |
| | 1 | 0.1083 | 0.1134 | 0.1190 | 0.1251 | 0.1104 | 0.1125 | 0.1147 |
| | 2 | 0.1181 | 0.1236 | 0.1296 | 0.1363 | 0.1203 | 0.1226 | 0.1250 |
| | 5 | 0.1472 | 0.1541 | 0.1617 | 0.1700 | 0.1500 | 0.1529 | 0.1560 |
| | 10 | 0.1959 | 0.2051 | 0.2151 | 0.2262 | 0.1996 | 0.2035 | 0.2075 |
| 5 | 0 | 0.2465 | 0.2580 | 0.2707 | 0.2846 | 0.2511 | 0.2560 | 0.2611 |
| | 1 | 0.2562 | 0.2682 | 0.2814 | 0.2959 | 0.2611 | 0.2661 | 0.2714 |
| | 2 | 0.2659 | 0.2784 | 0.2921 | 0.3071 | 0.2710 | 0.2762 | 0.2817 |
| | 5 | 0.2951 | 0.3090 | 0.3241 | 0.3408 | 0.3007 | 0.3065 | 0.3126 |
| | 10 | 0.3438 | 0.3599 | 0.3775 | 0.3970 | 0.3503 | 0.3571 | 0.3641 |
| 10 | 0 | 0.4930 | 0.5161 | 0.5414 | 0.5693 | 0.5023 | 0.5120 | 0.5221 |
| | 1 | 0.5027 | 0.5263 | 0.5520 | 0.5805 | 0.5122 | 0.5221 | 0.5324 |
| | 2 | 0.5124 | 0.5364 | 0.5627 | 0.5917 | 0.5221 | 0.5322 | 0.5428 |
| | 5 | 0.5416 | 0.5670 | 0.5948 | 0.6254 | 0.5519 | 0.5625 | 0.5737 |
| | 10 | 0.5903 | 0.6179 | 0.6482 | 0.6816 | 0.6014 | 0.6131 | 0.6252 |

The dimensionless fundamental frequencies $\Omega_d$ and relative damping ratio $\xi$ of the FGPNPs with various parameters of the GVF foundations is presented in Tables 4 and 5 for $\mu = 0$, and Tables 6 and 7 for $\mu = 4$. The results show that the increase of the damping coefficients $C_d, C_s$ leads to the reductions of the damped frequencies $\Omega_d$ of the FGPNPs, and the relative damping ratio $\xi$ increases. By comparisons of the local plates $(\mu = 0)$ and those of the nonlocal plates $(\mu = 4)$, it can be seen that the damped frequencies of the nonlocal plates are smaller than those of the local plates. It means the nonlocal parameters play softening roles in the vibration response of the FGPNPs.

Figure 2 presents how the damping coefficient $C_d$ influences on the damped vibration properties of the FGPNPs with $C_s = 10$, $K_w = 10,\ K_s = 5,\ \mu = 4,\ p = 1$. The damped frequencies $\Omega_d$ decrease when the damping coefficient $C_d$ increases. The reason is that when the damping coefficient $C_d$ increases, the dissipation of the vibration energy increases; therefore, the damping ratios $\xi$ increase, the period of the vibration increases, and the damped frequencies $\Omega_d$ decrease. When the damping coefficient reaches the critical point, the damping ratios $\xi$ equal 1 and the FGPNPs reach the critical state. Following the critical points, the FGPNPs undergo overdamped motion, it means the damped frequencies $\Omega_d$ equal 0, the damping ratios $\xi$ are greater than 1 and the real parts $\Omega_{Re}$ have two values as presented in Fig. 2(b). These two values denote two exponential decay rates, the energy dissipates rapidly, and no oscillation occurs, the nanoplate returns to equilibrium monotonically.

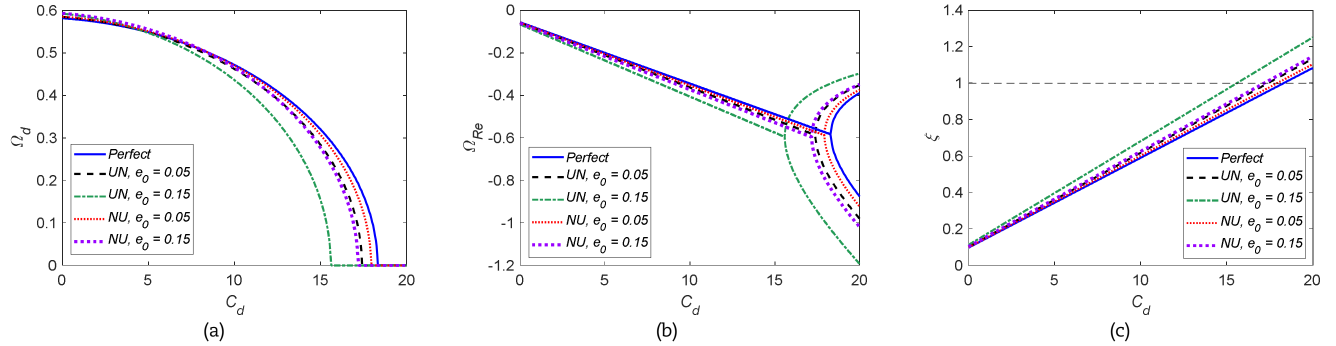


**Fig. 2.** The effects of damping coefficient $C_d$ on the vibration characteristics of FGPNPs, (a) $\Omega_d$ of the FGPNPs, (b) $\Omega_{Re}$ of the FGPNPs, (c) $\xi$ of the FGPNPs.

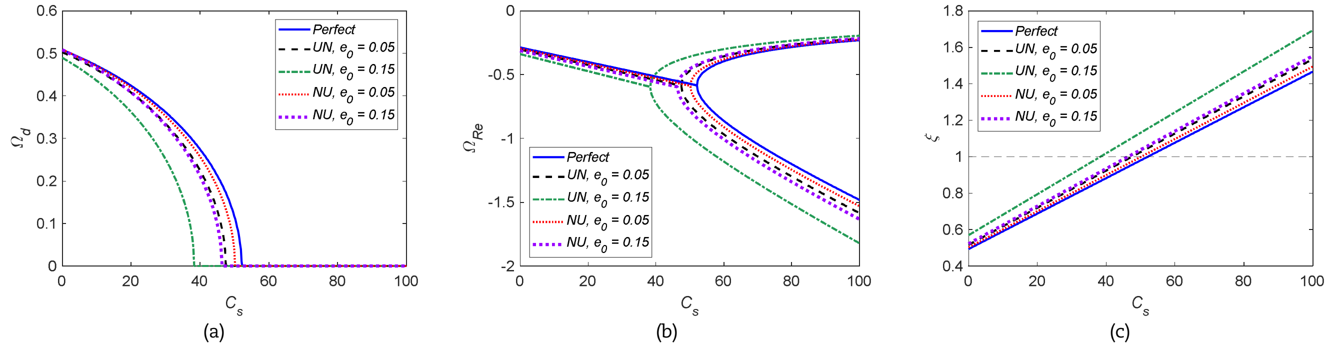


**Fig. 3.** The effects of damping coefficient $C_s$ on the vibration characteristics of FGPNPs, (a) $\Omega_d$ of the FGPNPs, (b) $\Omega_{Re}$ of the FGPNPs, (c) $\xi$ of the FGPNPs.

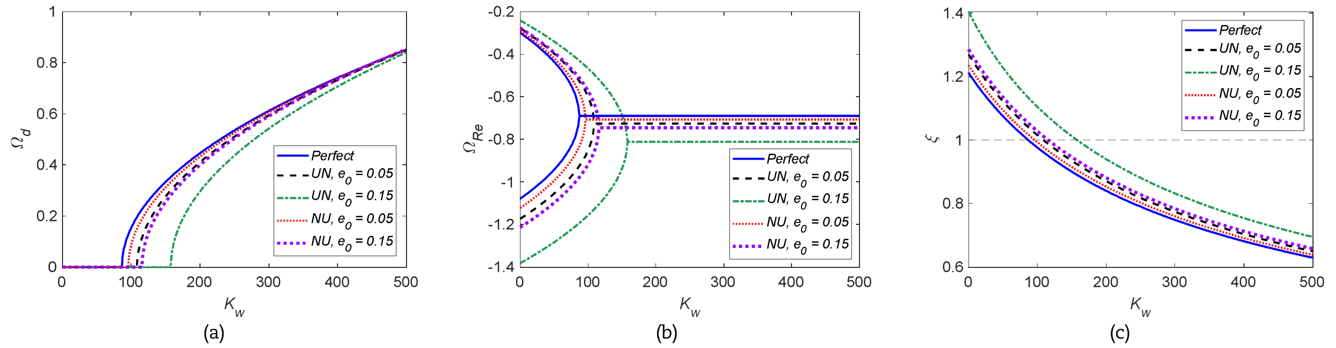


**Fig. 4.** The effects of stiffness $K_w$ on the vibration characteristics of the FGPNPs, (a) $\Omega_d$ of the FGPNPs, (b) $\Omega_{Re}$ of the FGPNPs, (c) $\xi$ of the FGPNPs.

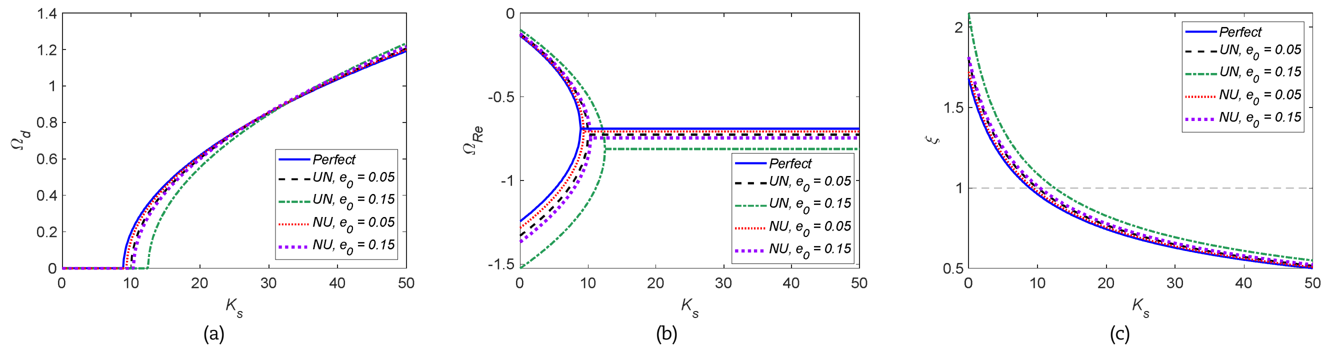


**Fig. 5.** The effects of shear stiffness $K_s$ on the vibration characteristics of the FGPNPs, (a) $\Omega_d$ of the FGPNPs, (b) $\Omega_{Re}$ of the FGPNPs, (c) $\xi$ of the FGPNPs.

The influences of the damping coefficient $C_s$ on the damped vibration characteristics are demonstrated in Fig. 3. In this example: $C_d = 10,\ K_w = 10,\ K_s = 5,\ \mu = 4,\ p = 1$. As presented in this figure, the effects of the damping coefficient $C_s$ are less than that of the damping coefficient $C_d$. The curve of the damped frequency is smooth and concave down. This means that when the damping coefficient $C_s$ increases, the damped frequencies $\Omega_d$ decrease, and the damping ratio $\xi$ increases. When the damping coefficient $C_s$ is small, the FGPNPs are subjected to underdamped vibration, it means the damped frequency $\Omega_d$ is greater than 0, the damping ratio $\xi$ is smaller than 1, and the real part $\Omega_{Re}$ has one value. At the critical state, the damped frequency equals 0, the damping ratio equals 1, and the curve of the real part splits into two branches, and the nanoplates transition from oscillatory to non-oscillatory motion. Following the critical point, the damped frequency equals 0, the damping ratio is greater than 1, and the real part has two values.

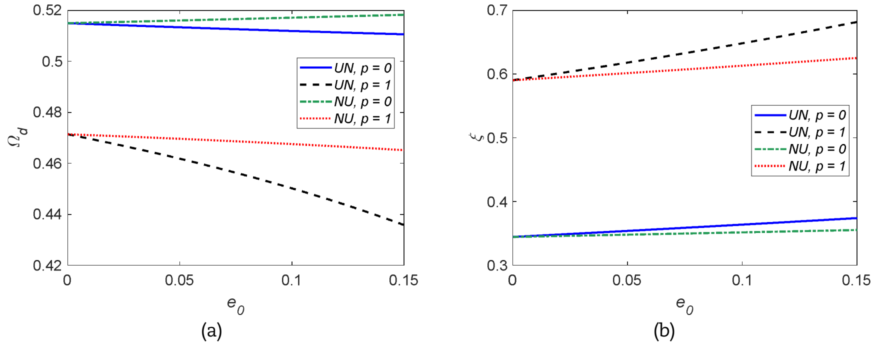


**Fig. 6.** The effects of porosity coefficient $e_0$ on the vibration characteristics of the FGPNPs, (a) $\Omega_d$ of the FGPNPs, (b) $\xi$ of the FGPNPs.

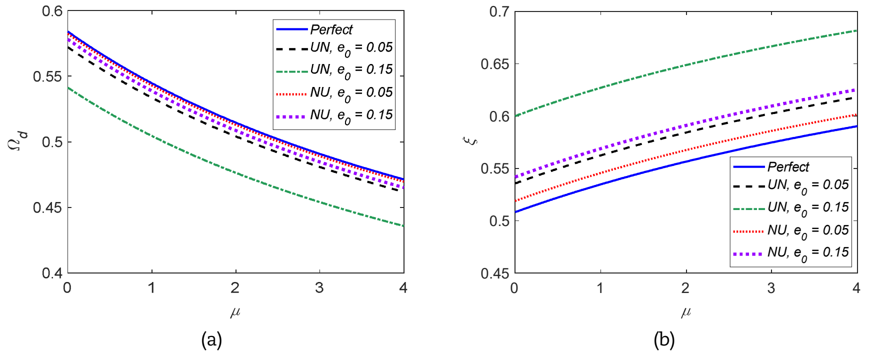


**Fig. 7.** The effects of nonlocal parameter $\mu$ on the vibration characteristics of the FGPNPs, (a) $\Omega_d$ of the FGPNPs, (b) $\xi$ of the FGPNPs.

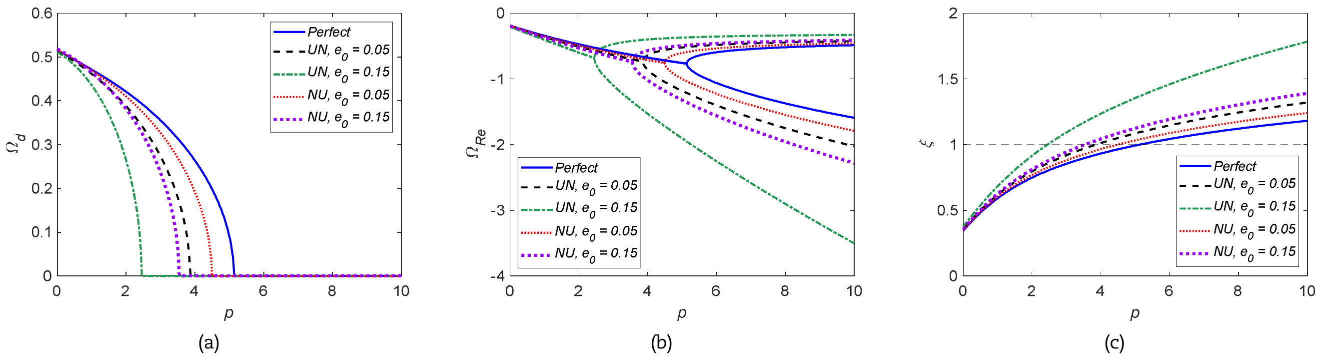


**Fig. 8.** The effects of index $p$ on the vibration characteristics of the FGPNPs, (a) $\Omega_d$ of the FGPNPs, (b) $\Omega_{Re}$ of the FGPNPs, (c) $\xi$ of the FGPNPs.

The investigation on the influences of the stiffness $K_w$ on the damped vibration properties of the FGPNPs was carried out on Fig. 4. In this examination: $C_d = 20,\ C_s = 20,\ K_s = 5,\ \mu = 4,\ p = 1.$ When the stiffness $K_w$ is small, the FGPNPs are under the overdamped motion. It means the damped frequency $\Omega_d$ equals 0, the damping ratio $\xi$ is larger than 1, and the real part $\Omega_{Re}$ has two values. When the stiffness $K_w$ rises over the critical point, the motion of the FGPNPs shifts from overdamped motion to underdamped vibration. At the underdamped vibration state, the damped frequency $\Omega_d$ increases when the stiffness $K_w$ increase. Figure 5 presents the effects of the stiffness $K_s$ on the damped vibration properties of the FGPNPs with $C_d = 20,\ C_s = 20,\ K_w = 10,\ \mu = 4,\ p = 1.$ It can be seen that the effects of the stiffness $K_s$ on the damped vibration of the FGPNPs are similar to the effects of the stiffness $K_w$, however, its influences are more significant than that of the stiffness $K_w$.

The influences of the porosity on the damped vibration characteristics of the FGPNPs are exhibited in Fig. 6 with two cases of power-law indexes $p = 0$ and $p = 1.$ In this example: with $C_d = 10,\ C_s = 10,\ K_w = 10,\ K_s = 5,\ \mu = 4.$ As presented in this figure, when the porosity coefficient, $e_0$, the behavior of the damped frequency can vary, either increasing or decreasing. When $p = 0,$ the damped frequency of the FGPNPs with UN porosity decreases, but the frequency of the FGPNPs with NU porosity increases as the increase of the porosity coefficients $e_0$. When $p = 1,$ the damped frequency of both UN and NU porosity distributions decreases as an increase of the porosity coefficient $e_0$. In summary, the effect of porosity on damped vibration behavior of FGPNPs is non-monotonic and case-dependent, it depends on the balance between stiffness and mass degradations.

Figure 7 illustrates the impacts of the nonlocal parameters on the damped vibration properties of the FGPNPs with $C_d = 10,$ $C_s = 10,\ K_w = 10,\ K_s = 5,\ p = 1.$ As can be seen from this figure, when the nonlocal parameter $\mu$ increases, the damped frequency of the FGPNPs decreases. The reason is that the nonlocal phenomenon makes the nanoplates softer than local ones.

The influence of the power-law index on the damped vibration of the FGPNPs with $C_d = 10,\ C_s = 10,\ K_w = 10,\ K_s = 5,\ \mu = 4,$ are presented in Fig. 8. At the underdamped state, when the power-law index $p$ increases, the damped frequency of the FGPNPs decreases rapidly, and reaches critical points. At the critical point, the damped frequency equals 0, and the damping ratio $\xi$ equals 1. The frequency of the FGPNPs following critical point, the frequency of the FGPNPs equal 0, the real part $\Omega_{Re}$ has two values and the damping ratio $\xi$ is higher than 1. In the physical view, when the power-law index $p$ increases, the volume fraction of ceramic decreases and that of metal increases; therefore, the stiffness of the FGPNPs decreases, leading to the decrease of the damped frequency.

## 6. Conclusion

In this study, a comprehensive study of the damped vibration characteristics of the functionally graded nanoplates was carried out focusing on the small-scale and porosity effects. Based on simple higher-order shear deformation and nonlocal elasticity theory, the governing equations of motion were established and then they are solved using Navier's solution. Based on the present results, the following remarkable conclusions should be drawn:

- When the damping coefficients are considered, the nanoplates are under damped vibration. The state of the vibration depends on the values of the damping coefficients.
- When the damping coefficients increase, energy dissipation increases, leading to a decrease in the damped frequency of the nanoplates.
- The stiffness of the foundation increases the total rigidity of the nanoplate-foundation system, consequently, the damped frequencies of the nanoplates increase.
- The effects of the porosity on the vibration behavior of the nanoplates differ from the porosity distributions, either increasing or decreasing.

The results of this study serve as a reference for the analysis, design, testing, and optimization of the nanostructures. The proposed viscoelastic foundation model should be employed for analysis of complex structures with arbitrary boundary conditions using new solution methodologies to overcome the limitations of Navier's method. The dynamic response of the nanostructures in contact with viscoelastic foundations should be an important aspect for future work.

## Author Contributions

L.T. Son planned the scheme, conducted the formal analysis and investigation, analyzed the results, and wrote the original draft; P.V. Vinh initiated the project, developed the mathematical modeling and examined the theory validation, and edited the final version of the article. The manuscript was written through the contribution of all authors. All authors discussed the results, reviewed, and approved the final version of the manuscript.

## Acknowledgments

Not Applicable.

## Conflict of Interest

The authors have no competing interests to declare.

## Funding

The authors received no financial support for this article.

## Data Availability Statements

All data was included in the article.

## References

[1] Russo C., Mocera F., Somà A., MEMS sensors for sport engineer applications, *IOP Conference Series: Materials Science and Engineering*, 1038(1), 2021, 12056.
[2] Fei, J., Ding, H., System Dynamics and Adaptive Control for MEMS Gyroscope Sensor, *International Journal of Advanced Robotic Systems*, 7(4), 2010, 29.
[3] Thai, H.T, Vo, T.P., Nguyen, T.K., Kim, S.E., A review of continuum mechanics models for size-dependent analysis of beams and plates, *Composite Structures*, 177, 2017, 196–219.
[4] Ghayesh, M.H., Farajpour, A., A review on the mechanics of functionally graded nanoscale and microscale structures, *International Journal of Engineering Science*, 137, 2019, 8-36.
[5] Reddy J.N., A General Nonlinear Third-Order Theory of Functionally Graded Plates, *International Journal of Aerospace and Lightweight Structures*, 1(1), 2011, 1-21.
[6] Liew, K.M., Lei, Z.X., Zhang, L.W., Mechanical analysis of functionally graded carbon nanotube reinforced composites: A review, *Composite Structures*, 120, 2015, 90-97.
[7] Saleh, B., Jiang, J., Fathi, R., Al-hababi, T., Xu, Q., Wang, L., Song, D., Ma, A., 30 Years of functionally graded materials: An overview of manufacturing methods, Applications and Future Challenges, *Composites Part B: Engineering*, 201, 2020, 108376.
[8] Swaminathan, K., Naveenkumar, D.T., Zenkour, A.M., Carrera, E., Stress, vibration and buckling analyses of FGM plates-A state-of-the-art review, *Composite Structures*, 120, 2015, 10-31.
[9] Chen, D., Gao, K., Yang, J., Zhang, L., Functionally graded porous structures: Analyses, performances, and applications - A Review, *Thin-Walled Structures*, 191, 2023, 111046.
[10] Wu, C.P., Liu, Y.C., A review of semi-analytical numerical methods for laminated composite and multilayered functionally graded elastic/piezoelectric plates and shells, *Composite Structures*, 147, 2016, 1-15.
[11] Eringen, A.C., Linear theory of nonlocal elasticity and dispersion of plane waves, *International Journal of Engineering Science*, 10, 1972, 425-435.
[12] Eringen, A.C., On differential equations of nonlocal elasticity and solutions of screw dislocation and surface waves, *Journal of Applied Physics*, 54, 1983, 4703-4710.
[13] Eringen, A.C., Edelen, D.G.B., On nonlocal elasticity, *International Journal of Engineering Science*, 10, 1972, 233–248.
[14] Lal, R., Ahlawat, N., Buckling and vibration of functionally graded non-uniform circular plates resting on Winkler foundation, *Latin American Journal of Solids and Structures*, 12, 2015, 2231-2258.
[15] Sobhani, E., Avcar, M., Natural frequency analysis of imperfect GNPRN conical shell, cylindrical shell, and annular plate structures resting on Winkler-Pasternak Foundations under arbitrary boundary conditions, *Engineering Analysis with Boundary Elements*, 144, 2022, 145-164.
[16] Jiang, J., Lian, C., Meng, B., King, H., Wang, J., An Approximate Solution of the Bending of Beams on a Nonlinear Elastic Foundation with the Galerkin Method, *Journal of Applied and Computational Mechanics*, 11(2) 2025, 285-293.
[17] Assie, A.E., Mohamed, S.A., Shanab, R.A., Abo-bakr, R.M., Eltaher, M.A., Static Buckling of 2D FG Porous Plates Resting on Elastic Foundation based on Unified Shear Theories, *Journal of Applied and Computational Mechanics*, 9(1), 2023, 239-258.
[18] Ipek, C., Sofiyev, A.H., Fantuzzi, N., Efendiyeva, S.P., Buckling Behavior of Nanocomposite Plates with Functionally Graded Properties under Compressive Loads in Elastic and Thermal Environments, *Journal of Applied and Computational Mechanics*, 9(4), 2023, 974-986.
[19] Daikh, A.A., Zenkour, A.M., Bending of Functionally Graded Sandwich Nanoplates Resting on Pasternak Foundation under Different Boundary

Conditions, *Journal of Applied and Computational Mechanics*, 6, 2020, 1245-1259.
[20] Pour M.A., Golmakani M.E., Malikan M. Thermal Buckling Analysis of Circular Bilayer Graphene Sheets Resting on an Elastic Matrix Based on Nonlocal Continuum Mechanics, *Journal of Applied and Computational Mechanics*, 7(4), 2021, 1862-1877.
[21] Driz, H., Attia, A., Bousahla, A.A., Addou, F.Y., Bourada, M., Tounsi, A., et al., Dynamic response of imperfect functionally graded plates: Impact of graded patterns and viscoelastic foundation, *Structural Engineering and Mechanics*, 91(6), 2024, 551-565.
[22] Tounsi, A., Bousahla, A.A., Tahir, S.I., Mostefa, A.H., Bourada, F., Al-Osta, M.A., et al., Influences of Different Boundary Conditions and Hygro-Thermal Environment on the Free Vibration Responses of FGM Sandwich Plates Resting on Viscoelastic Foundation, *International Journal of Structural Stability and Dynamics*, 24(11), 2023, 2450117.
[23] Van Vinh, P., Sedighi, H.M., Civalek, Ö., A comprehensive study on the critical damping characteristics of vibrating functionally graded sandwich plates with general visco-Winkler–Pasternak foundations, *Archives of Civil and Mechanical Engineering*, 25, 2025, 101.
[24] Zhang, S., Wang, M., Chen, C., Shahsavari, D., Karami, B., Tounsi A., Wave propagation in carbon nanotube-reinforced nanocomposite doubly-curved shells resting on a viscoelastic foundation, *Waves in Random and Complex Media*, 35(2), 2022, 4105-4128.
[25] Foroutan, K., Ahmadi, H., Nonlinear vibration of SSMFG cylindrical shells with internal resonances resting on the nonlinear viscoelastic foundation, *Structural Engineering and Mechanics*, 84(6), 2022, 767-782.
[26] Li, Z., Liu, J., Hu, B., Wang, Y., Shen, H., Wave propagation analysis of porous functionally graded piezoelectric nanoplates with a visco-Pasternak foundation, *Applied Mathematics and Mechanics (English Edition)*, 44, 2023, 35-52.
[27] Mouaici, F., Benyoucef, S., Atmane, H.A., Tounsi, A., Effect of porosity on vibrational characteristics of non-homogeneous plates using hyperbolic shear deformation theory, *Wind and Structures, An International Journal*, 22(4), 2016, 429-454.
[28] Wang, Z.Z., Wang, T., Ding, Y.M., Ma, L.S., Free vibration analysis of functionally graded porous plates based on a new generalized single-variable shear deformation plate theory, *Archive of Applied Mechanics*, 93, 2023, 2549-2564.
[29] Ghazwani, M.H., Alnujaie, A., Vinh, P.V., Assessment of the porosity and general viscoelastic foundation effects on the damped vibration analysis of functionally graded plates, *Mechanics Based Design of Structures and Machines*, 2025, 1-26.
[30] Zenkour, A.M., A novel mixed nonlocal elasticity theory for thermoelastic vibration of nanoplates, *Composite Structures*, 185, 2018, 821-833.
[31] Hoa, L.K., Vinh, P.V., Duc, N.D., Trung, N.T., Son, L.T., Thom, D.V., Bending and free vibration analyses of functionally graded material nanoplates via a novel nonlocal single variable shear deformation plate theory, *Proceedings of the Institution of Mechanical Engineers, Part C: Journal of Mechanical Engineering Science*, 235(18), 2021, 3641-3653.
[32] Coskun, S., Kim, J., Toutanji, H., Bending, free vibration, and buckling analysis of functionally graded porous micro-plates using a general third-order plate theory, *Journal of Composites Science*, 3(1), 2019, 15.

## ORCID iD

Le Truong Son https://orcid.org/0000-0003-3019-4291
Pham Van Vinh https://orcid.org/0000-0002-8053-6977



**How to cite this article:** Son L.T., Vinh P.V. Effects of Porosity and Nonlocality on the Damped Vibration Behaviors of Functionally Graded Rectangular Nanoplates on General Viscoelastic Medium, *J. Appl. Comput. Mech.*, 12(1), 2026, 226-237. https://doi.org/10.22055/jacm.2025.48328.5152